



**HAL**  
open science

## Heat as a tracer for understanding transport processes in fractured media: Theory and field assessment from multiscale thermal push-pull tracer tests

Maria V. Klepikova, Tanguy Le Borgne, Olivier Bour, Marco Dentz, Rebecca Hochreutener, Nicolas Lavenant

### ► To cite this version:

Maria V. Klepikova, Tanguy Le Borgne, Olivier Bour, Marco Dentz, Rebecca Hochreutener, et al.. Heat as a tracer for understanding transport processes in fractured media: Theory and field assessment from multiscale thermal push-pull tracer tests. *Water Resources Research*, 2016, 52 (7), pp.5442-5457. 10.1002/2016WR018789 . insu-01346041

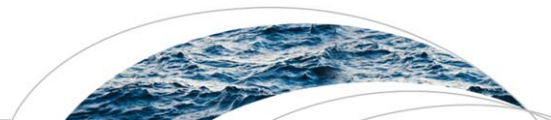
**HAL Id: insu-01346041**

**<https://insu.hal.science/insu-01346041>**

Submitted on 20 Jul 2016

**HAL** is a multi-disciplinary open access archive for the deposit and dissemination of scientific research documents, whether they are published or not. The documents may come from teaching and research institutions in France or abroad, or from public or private research centers.

L'archive ouverte pluridisciplinaire **HAL**, est destinée au dépôt et à la diffusion de documents scientifiques de niveau recherche, publiés ou non, émanant des établissements d'enseignement et de recherche français ou étrangers, des laboratoires publics ou privés.



## RESEARCH ARTICLE

10.1002/2016WR018789

### Key Points:

- Flow channeling in fractured media is shown to have a significant effect on the scale dependency of heat recovery
- Thermal push-pull tracer tests are shown to provide valuable insights on fracture geometry and fracture aperture
- The multichannel fracture model was found to provide an excellent match with the observed temperature breakthrough curves at multiple scales

### Correspondence to:

K. Maria,  
maria.klepikova@erdw.ethz.ch

### Citation:

Klepikova, M. V., T. Le Borgne, O. Bour, M. Dentz, R. Hochreutener, and N. Lavenant (2016), Heat as a tracer for understanding transport processes in fractured media: Theory and field assessment from multiscale thermal push-pull tracer tests, *Water Resour. Res.*, 52, doi:10.1002/2016WR018789.

Received 16 FEB 2016

Accepted 22 JUN 2016

Accepted article online 24 JUN 2016

# Heat as a tracer for understanding transport processes in fractured media: Theory and field assessment from multiscale thermal push-pull tracer tests

**Maria V. Klepikova<sup>1,2</sup>, Tanguy Le Borgne<sup>1</sup>, Olivier Bour<sup>1</sup>, Marco Dentz<sup>3</sup>, Rebecca Hochreutener<sup>1,4</sup>, and Nicolas Lavenant<sup>1</sup>**

<sup>1</sup>Géosciences Rennes, OSUR, UMR CNRS 6118, University of Rennes 1, Rennes, France, <sup>2</sup>ETH Zurich, Geological Institute, Zurich, Switzerland, <sup>3</sup>Spanish National Research Council (IDAEA-CSIC), Barcelona, Spain, <sup>4</sup>OSU, Biological and Ecological Engineering, Corvallis, Oregon, USA

**Abstract** The characterization and modeling of heat transfer in fractured media is particularly challenging as the existence of fractures at multiple scales induces highly localized flow patterns. From a theoretical and numerical analysis of heat transfer in simple conceptual models of fractured media, we show that flow channeling has a significant effect on the scaling of heat recovery in both space and time. The late time tailing of heat recovery under channeled flow is shown to diverge from the  $T(t) \propto t^{-1.5}$  behavior expected for the classical parallel plate model and follow the scaling  $T(t) \propto 1/t(\log t)^2$  for a simple channel modeled as a tube. This scaling, which differs significantly from known scalings in mobile-immobile systems, is of purely geometrical origin: late time heat transfer from the matrix to a channel corresponds dimensionally to a radial diffusion process, while heat transfer from the matrix to a plate may be considered as a one-dimensional process. This phenomenon is also manifested on the spatial scaling of heat recovery as flow channeling affects the decay of the thermal breakthrough peak amplitude and the increase of the peak time with scale. These findings are supported by the results of a field experimental campaign performed on the fractured rock site of Ploemeur. The scaling of heat recovery in time and space, measured from thermal breakthrough curves measured through a series of push-pull tests at different scales, shows a clear signature of flow channeling. The whole data set can thus be successfully represented by a multichannel model parametrized by the mean channel density and aperture. These findings, which bring new insights on the effect of flow channeling on heat transfer in fractured rocks, show how heat recovery in geothermal tests may be controlled by fracture geometry. In addition, this highlights the interest of thermal push-pull tests as a complement to solute tracers tests to infer fracture aperture and geometry.

## 1. Introduction

The characterization and predictive modeling of heat transfer processes in fractured media is of central interest for the development of conventional and enhanced geothermal systems, as well as Aquifer Thermal Energy Storage (ATES) [e.g., Kolditz, 1995; Genter et al., 2003; Kocabas, 2005; Saar, 2011]. It is also important for interpreting temperature anomalies to infer subsurface flows and surface-groundwater exchanges, which has recently gained popularity in particular through the development of distributed fiber optic temperature sensing methods [e.g., Anderson, 2005; Saar, 2011; Vogt et al., 2010; Jung and Pruess, 2012; Selker et al., 2006; Irvine et al., 2015]. Heat transfer in fractured media is governed by heterogeneous structures at different scales. At the fracture scale, the distribution of apertures controls the distribution of advective fluxes that disperses heat in the medium. Fracture roughness also determines the geometry of the fracture-matrix interface and therefore the efficiency of diffusive exchange processes [Neuville et al., 2010]. At network scale, the distribution of fracture lengths and their spatial organization determines the geometry and connectivity of preferential flowpaths that control the fate of heat plumes [Geiger and Emmanuel, 2010]. These different sources of complexity render the characterization and modeling of heat transfer in fractured media a challenging task.

Transport processes in fractured media generally exhibit anomalous features that manifest themselves on tracer breakthrough curves as fast initial breakthrough times and long tailing in late time recovery [Haggerty

*et al.*, 2000; *Becker and Shapiro*, 2000, 2003; *Kang et al.*, 2015]. Since heat diffusivity is much larger than solute diffusivity, heat transfer processes may be more sensitive to fracture-matrix diffusion processes than advective dispersion processes [e.g., *Lauwerier*, 1955; *Kocabas and Horne*, 1990; *Gringarten and Sauty*, 1975; *Pruess and Doughty*, 2010; *Jung and Pruess*, 2012; *Read et al.*, 2013]. Despite this, numerical simulations in fracture networks have shown that heterogeneous advection processes have a significant impact on heat transfer [*Geiger and Emmanuel*, 2010]. This motivates us to investigate the signature of fracture heterogeneity on heat transfer processes, with the objective of understanding what can be learned from fractured media heterogeneity from thermal tracer tests.

The analysis of the late-time behavior of tracer breakthrough curves can reveal the nature of transport phenomena that control the longest residence times in heterogeneous media [*Haggerty et al.*, 2000; *Becker and Shapiro*, 2000, 2003; *Le Borgne and Gouze*, 2008; *Kang et al.*, 2015]. Conservative, nonreacting solute tracer tests conducted in fractured media often display power-law late time tailing  $\propto t^{-\beta}$  for the solute breakthrough curve, that manifests as a straight line in double logarithmic plots. The power law slope of the breakthrough tailing, characteristic of non-Fickian dispersion processes, has been related to heterogeneous advection and multirate mass transfer processes [e.g., *Haggerty et al.*, 2001; *Carrera et al.*, 1998; *Dentz and Berkowitz*, 2003; *Becker and Shapiro*, 2003; *Gouze et al.*, 2008a,b; *Le Borgne and Gouze*, 2008; *Kang et al.*, 2015]. Diffusion processes between the immobile and the water-flowing medium fractions are known to produce power-law breakthrough behavior  $\propto t^{-\beta}$  for solute concentration or temperature. For diffusion in a homogeneous matrix, the expected power law exponent is  $\beta = 3/2$  [*Maloszewski and Zuber*, 1985; *Haggerty and Gorelick*, 1995; *Tsang*, 1995]. Considering a heterogeneous matrix domain, different exponents  $\beta$  can be obtained and modeled in the framework of multirate mass transfer [*Haggerty et al.*, 1995, 2000; *Carrera et al.*, 1998; *Gouze et al.*, 2008a,b]. Here we investigate the role of heterogeneity in the fracture plane on the tailing exponent  $\beta$ , while the matrix is kept homogeneous. In particular, we show that flow channeling leads to a late time temporal scaling of heat recovery, which has not been previously described.

This phenomenon is expected to impact the scale dependency of heat recovery in thermal tracer tests. To verify this, we conducted a series of thermal push-pull tests at the fractured crystalline rock of the Ploemur experimental site (H+ network, France, Figure 4a). Push-pull tracer tests, which maximize recovery by injection and subsequent recovery from the same location, are well adapted to study fracture-matrix exchange processes, which are irreversible upon flow inversion [e.g., *Hosanski and Ledoux*, 1982; *Becker and Shapiro*, 2003; *Neretnieks*, 2007; *Gouze et al.*, 2008b; *Le Borgne and Gouze*, 2008; *Kang et al.*, 2015]. The scale of investigation can be varied by changing the push time [e.g., *Le Borgne and Gouze*, 2008]. The use of push-pull heat tracer tests in fractured media was recently investigated by the analytical study of *Jung and Pruess* [2012]. They developed an analytical solution for thermal push-pull tests, using an idealized model that considers fractures as parallel-plate systems with a constant aperture. For a given thermal test, the recovered thermal breakthrough curve was found to be insensitive on flow rate and weakly sensitive to aperture. Here we take a different approach by analyzing of the scaling of heat recovery with the investigation volume for different push times, and the temporal decay of late time heat recovery. As discussed in the following the observed scale effects provide strong constraints on the impact of fracture flow heterogeneity on heat transfer process and on fracture properties.

The paper is organized as follows. In section 2, we present the different conceptual models that we consider for fracture matrix exchange and we derive analytically the expected temporal scaling for heat recovery. In section 3, we describe the numerical models that we use to simulate heat transfer for these different conceptual models of fracture matrix exchange. In section 4, we present the experimental site and the thermal push-pull tracer tests data set. Finally, in section 5, we discuss the spatial and temporal scaling of heat recovery in fractured media based on the interpretation of field data and numerical simulations, in the light of the theoretical predictions of section 2.

## 2. Conceptual Models of Fracture-Matrix Exchanges and Associated Temporal Scalings

To investigate the impact of flow heterogeneity within fracture planes on heat exchange processes we consider different conceptual models that represent the two end-members of no channeling and extreme channeling.

2.1. Conceptual Models

“Parallel plate” models, which disregard fracture roughness, are widely used for modeling heat transport in fractures [e.g., *Lauwerier, 1955; Bodvarsson and Tsang, 1982; Jung and Pruess, 2012; Molson et al., 2007*]. Yet aperture fluctuations in fracture planes can produce significant flow channeling [*Gylling et al., 1999; Becker and Shapiro, 2003*], which affects heat transfer with the matrix because of the reduction of effective exchange area [*Neuville et al., 2010*]. Here we consider simplified models of channeled flow composed of one or several cylinders (Figure 1). As heat is transported advectively in the fracture the main heat fluxes are oriented in the direction perpendicular the fracture-matrix interface. Hence, for the parallel plate model, heat fluxes during heating and recovery are all oriented along the same direction, perpendicular to the fracture plane. On the other hand, for the channel model, heat diffuses radially outward from the channel to the matrix during heating and radially inward from the matrix to the channel during recovery. Heat fluxes are thus oriented in all possible directions within the plane perpendicular to the channel. Effectively heat fluxes are thus mostly one-dimensional for the “parallel plate” model and two-dimensional for the “channel” model. As discussed in the following this has significant effect on the spatial and temporal scaling of heat recovery. In the multichannel model heat diffusion profiles from each channel can superimpose each other

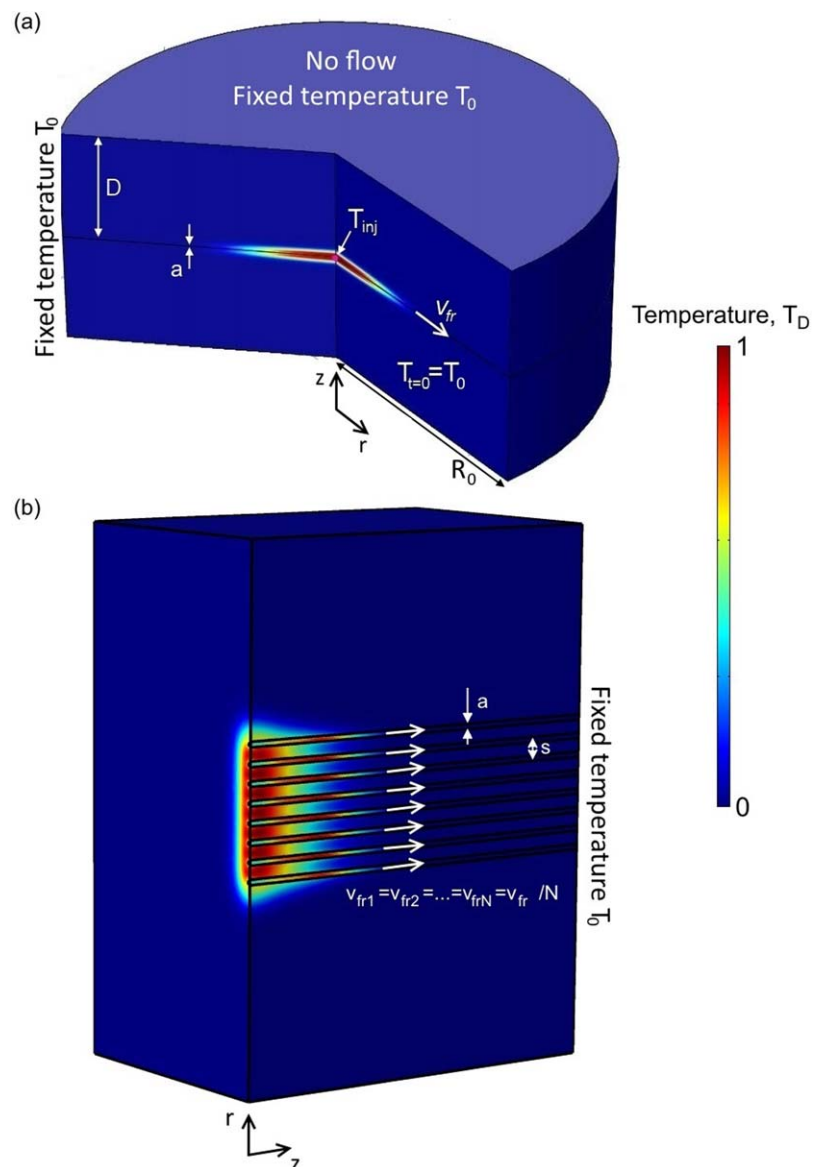


Figure 1. Conceptual models of fracture-matrix exchange: (a) parallel plates geometry, (b) channel, and (c) multichannel geometries.

thus affecting thermal response. Figure 1 summarizes all types of fracture geometry concepts used in this study: parallel plate model (a), “channel” (b) and “multichannel” fracture geometries (c).

### 2.2. Temporal Scaling of Heat Recovery

When immobile zones are embedded into a mobile domain, it has been shown that the particular geometry of immobile zones (e.g., plates, cylinders, spheres) do not affect the late-time scaling of concentration recovery, which is expected to follow the law  $c(t) \propto t^{-3/2}$  [Haggerty et al., 2000]. However, this has not been investigated for the case of mobile regions embedded in an immobile domain, which corresponds to the conceptual models discussed above. To characterize the effect of the dimensionality of heat fluxes on the late-time scaling of heat recovery, we consider a mobile-immobile model for heat transfer between mobile and immobile domains. Note that the following discussion is equally valid for solute transport. For convenience of the reader, we briefly recall the modeling equations and underlying assumptions. The fracture is represented by a cylindrical channel, see Figure 1, which exchanges heat with the surrounding matrix. Average heat transfer in the mobile domain is described by

$$\phi_f \frac{\partial T_f}{\partial t} + \phi_r \frac{\partial T_r}{\partial t} = \frac{\lambda_f}{\rho_f C_{pf}} \frac{\partial^2 T_f}{\partial z^2} - q \frac{\partial T_f}{\partial z} \quad (1)$$

where  $\phi_f$  and  $\phi_r$  are the porosities of the fracture and matrix domains, respectively. The density, the thermal conductivity and the heat capacity in the mobile fracture domain are denoted by  $\rho$ ,  $\lambda_f$  and  $C_{pf}$ , respectively.  $T_f$  represents the cross-sectional average fluid temperature in the fracture

$$T_f(z, t) = \frac{2}{r_f^2} \int_0^{r_f} dr r g_f(r, z, t), \quad (2)$$

where  $g_f(r, z, t)$  denotes the heat distribution across the fracture.  $T_r$  is a bulk temperature in the rock matrix defined by

$$T_r(z, t) = \frac{2}{r_r^2} \int_{r_f}^{\infty} dr r g_r(r, z, t), \quad (3)$$

where  $g_r(r, z, t)$  denotes the heat distribution in the matrix. It is governed by the radial diffusion equation

$$\phi_r \frac{\partial g_r(r, z, t)}{\partial t} = \frac{\lambda_r}{r} \frac{\partial}{\partial r} r \frac{\partial}{\partial r} g_r(r, z, t), \quad (4)$$

where  $\lambda_r$  the thermal conductivity in the matrix domain.  $\mathbf{r}$  denotes the coordinate vector in the coordinate system attached to the immobile matrix domain. The initial condition here is  $g_r(r, z, t=0) = 0$ . The boundary conditions are  $g_r(r=r_f, z, t=0) = T_f(z, t)$  at the fracture matrix interface and 0 at  $r = \infty$ . Note that in accordance with other multirate mass transfer representations of heat and solute transport [Haggerty and Gorelick, 1995; Carrera et al., 1998], we assume that cross-sectional equilibrium is attained fast, which justifies the boundary condition at the interface, and axial heat transfer is negligible, which justifies the purely radial diffusion in the matrix described by (4). For a heterogeneous matrix, the memory function  $\varphi(t)$  is obtained analogously from the solution of a heterogeneous diffusion problem in the immobile matrix [Gouze et al., 2008a].

The solution of (4) can be expressed in terms of the Green’s function  $G(r, t)$ , which solves (4) for the boundary condition  $G(r=r_f, t) = \delta(t)$ , as

$$g_r(r, z, t) = \int_0^t dt' G(r, t-t') T_f(z, t'). \quad (5)$$

Thus, we obtain for  $T_r(z, t)$  by using (3)

$$T_r = \int_0^t dt' \varphi(t-t') T_f(\mathbf{x}, t'). \quad (6)$$

where we defined the memory function

$$\varphi(t) = \frac{2}{r_f^2} \int_{r_f}^{\infty} dr r G(r, t). \quad (7)$$

The solution of (4) for the Green's function can be obtained conveniently in Laplace space [Abramowitz and Stegun, 1972] as

$$\hat{G}(r, s) = \frac{K_0(\sqrt{s/\lambda_r} r)}{K_0(\sqrt{s/\lambda_r} r_f)}. \quad (8)$$

where  $K_i(r)$  is the modified Bessel function of the second kind [Abramowitz and Stegun, 1972]. The Laplace variable is  $s$ , the Laplace transform is marked by a hat. Thus, from (7), we obtain for the Laplace transform of  $\varphi(t)$

$$\hat{\varphi}(s) = \frac{1}{\sqrt{s\tau_r}} \frac{K_1(\sqrt{s\tau_r})}{K_0(\sqrt{s\tau_r})}, \quad (9)$$

where we defined  $\tau_r = r_f^2/\lambda_r$ , the time for heat transfer over a distance equal to the fracture radius. The behavior of  $\hat{\varphi}(s)$  behave at small  $s$  (which corresponds to large times) as

$$\hat{\varphi}(s) \propto -\frac{1}{\ln(s)}. \quad (10)$$

This Laplace space behavior corresponds to the following long time behavior of the memory function

$$\varphi(t) \propto \frac{1}{\ln(t)}. \quad (11)$$

We consider now the consequence of this scaling for the scaling of the breakthrough curves.

For a pulse injection, the breakthrough behavior at times that are large compared to the peak breakthrough time  $t_p$  is essentially given by the flux that emerges from the immobile zone [Haggerty et al., 2000] between the injection and detection points. The immobile  $T_r$  given by (3) can then be approximated for times  $t \gg t_p$  as

$$T_r \approx \varphi(t - t_p) A, \quad A = \int_0^{\infty} dt' T_f(z, t') \quad (12)$$

because  $T_f$  is peaked about  $t = t_p$ . Thus, the flux  $j_r(t) = -2\pi r_f \lambda_r \partial g_r(r_f, z, t) / \partial r$  emerging from the matrix is given by

$$j_r(t) = -\phi_r \pi r_f^2 \frac{\partial T_r}{\partial t} \propto -\frac{d\varphi(t)}{dt} \quad (13)$$

Note that we consider  $t \gg t_p$ . Thus, the long-time tailing behavior of the breakthrough curve can be fully understood in terms of the tailing behavior of the memory function  $\varphi(t)$ .

For the parallel plate model, heat transfer in the matrix is essentially a  $d = 1$  dimensional process. The memory function in this case scales as  $\varphi(t) \propto t^{-1/2}$  [Haggerty and Gorelick, 1995; Carrera et al., 1998]. The flux and thus the breakthrough curve in this case scales as  $j_r(t) \propto t^{-3/2}$ , which is the characteristic tailing behavior related to diffusion into a homogeneous matrix domain [Tsang, 1995; Hadermann and Heer, 1996].

This is quite different in the channel scenario. Here the interface between the mobile fracture channel and the immobile rock matrix represents an internal boundary of the immobile domain. Note that again, the heat flux from the matrix to the fracture is perpendicular to the channel, which now, however, is of dimension  $d = 2$ . The return process to the channel is now the radial diffusion process (4). By using (11) in (13), we obtain for the flux

$$j_r(t) \propto \frac{1}{t \ln(t)^2}, \quad (14)$$

which is the expected long-time scaling of the breakthrough curve. It is interesting to note that the derivative of the memory function is equal to the residence time distribution, or return time distribution

$p_r(t) \equiv -d\varphi(t)/dt$  of diffusing particles that are released at the fracture-rock matrix interface [Dentz et al., 2015; Comolli et al., 2016]. In fact, the behavior (14) is the same as the one found for the return probability in  $d = 2$  dimensions [Redner, 2001].

Hence, the dimensionality of the relevant diffusive flux is found to have a significant impact on tailing behavior in matrix diffusion systems. For  $d = 1$  dimensional diffusion perpendicular to the fracture-rock interface, the breakthrough curve shows the characteristic  $\propto t^{-3/2}$  behavior, while for radial diffusion it scales as  $\propto \frac{1}{\ln(t)^2}$ . Interestingly this result has not been reported before in the hydrology literature and it may therefore find applications for solute transport beyond heat transfer problems. For temperature recovery, this implies that the plate and channel models are expected to differ in terms of breakthrough curve tailing. In the following, we test these theoretical findings from numerical simulations and heat tracer test experiments in the field.

### 3. Numerical Modeling

To investigate further the temporal and spatial scaling of heat recovery and characterize its sensitivity to fracture aperture and geometry, we develop a numerical model of flow and heat transport using COMSOL Multiphysics as detailed in the following.

#### 3.1. Parallel Plate Model

The model geometry for a parallel plate fracture is illustrated in Figure 2a. Due to the axial-symmetry for a “plate” fracture geometry we model a 2-D domain, bounded by the fracture inlet, at radial distance  $r = 0$ , and a radial distance  $r = R_0$ , which is chosen far enough not to influence thermal breakthrough curves. The flow  $q$  within the parallel plate fracture with uniform aperture  $a$  is 2-D radial with a parabolic velocity transverse to the flow direction

$$q(r, z) = \frac{3Qz}{\pi r a} \left(1 - \frac{z}{a}\right), \tag{15}$$

where  $Q$  is the fluid injection rate. To model heat transport, we consider heat conduction in the matrix and in the fracture, and heat advection in the fracture. For the parallel plate fracture geometry, the governing equation for thermal transport in the system can be written as follows:

$$\rho_f C_{pf} \frac{\partial T_f}{\partial t} + \rho_f C_{pf} q(r, z) \frac{\partial T_f}{\partial r} - \lambda_f \frac{\partial^2 T_f}{\partial z^2} - \lambda_f \frac{\partial^2 T_f}{\partial r^2} = 0 \tag{16}$$

$$\rho_r C_{pr} \frac{\partial T_r}{\partial t} - \lambda_r \frac{\partial^2 T_r}{\partial z^2} - \lambda_r \frac{\partial^2 T_r}{\partial r^2} = 0 \tag{17}$$

where  $\rho$  is the density,  $C_p$  is the heat capacity,  $\lambda$  is the thermal conductivity and  $f$  and  $r$  subscripts denote fracture and rock correspondingly. At the interface between fracture and rock matrix, we have heat and flux

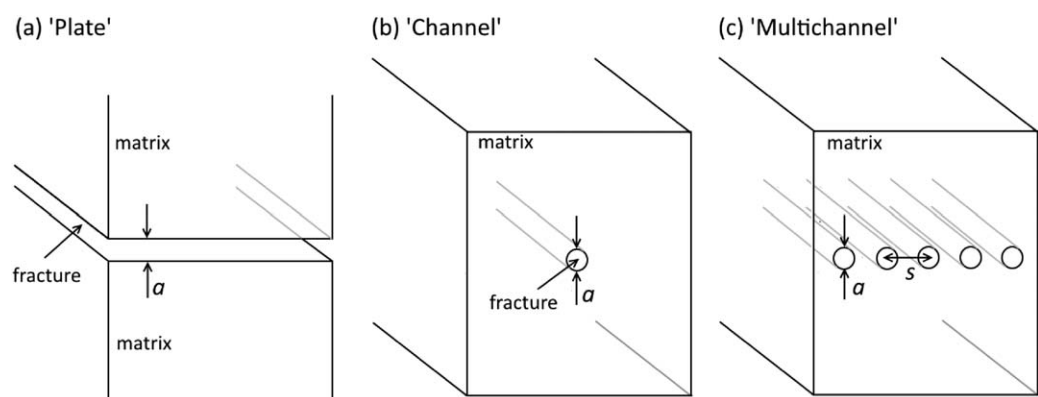


**Figure 2.** 3-D sketch for a (a) “plate” and (b) “multichannel” fracture models with parameter definitions.  $r$  direction is along the fracture hydraulic flow  $v_{fr}$ .  $a$  is the fracture aperture.  $T_0$  is the initial temperature of the rock matrix, supposed to be homogeneous and constant,  $T_{inj}$  is the fluid temperature at the fracture inlet(s).

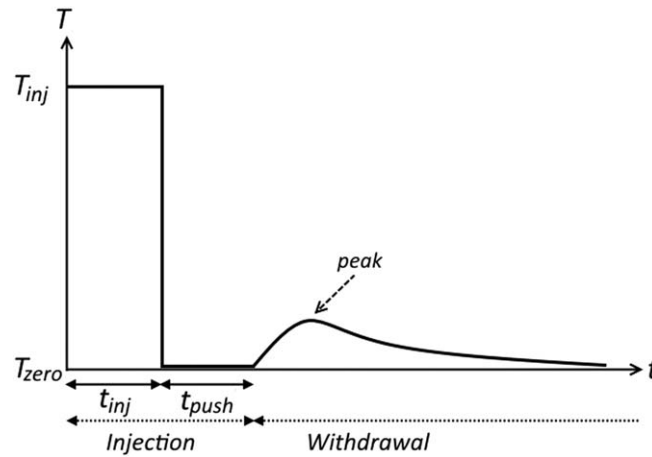


**Figure 3.** Typical push-pull breakthrough curve. The thermal tracer of temperature  $T_{inj}$  is injected during the time of injection  $t_{inj}$  and then is pushed with water of ambient temperature  $T_0$  during the push time  $t_{push}$ . Afterward, the tracer is pumped out.

continuity. The thermal tracer of temperature  $T|_{t=0} = T_{inj}$  is injected through the fracture inlet at the axis of the symmetry of the system during the time of injection  $t_{inj}$ . Afterward, the tracer is pushed with water of ambient temperature  $T|_{t=t_{inj}} = T_0$ . Following the experimental protocol, the push time is taken equal to the injection time  $t_{push} = t_{inj}$ . After flow reversal, the tracer is pumped out from the same point where the simulated thermal breakthrough recovery can be compared to the experimental breakthrough curves (Figure 3). Note, that once withdrawal begins, the boundary condition at the fracture inlet is changed to a “thermal insulation” boundary condition. The rock temperature at the outer boundaries as well the

boundary condition at fracture outlet is taken as  $T_0$ . In the example of Figure 2 the fracture aperture is  $a = 2$  mm, the thickness of the rock matrix layer is  $D = 3$  m. Here and below we used matrix thermal properties corresponding to the values measured on core samples from the experimental site. Water heat capacity is  $C_{pf} = 4189$  J/kgK and the density is  $\rho_f = 1000$  kg/m<sup>3</sup> [Incropera and DeWitt, 1996]. Density effects are not considered in the simulations since our primary goal is to analyze the impact of coupled flow channeling and heat diffusion.

### 3.2. Channel Model

For the “channel” and “multichannel” fracture geometries (Figure 1) we model 3-D cylindrical tubes with a constant flow velocity  $v_{fr}$  (Figure 2b). For the “multichannel” model flow partitions equally between  $N$  channels, reducing flow in each fracture to  $v_{fr}/N$ , where  $N$  is the number of channels. For the “channel” fracture geometry, radial symmetry to the modeled domain was assumed, and the governing equation for thermal transport is:

$$\rho_f C_{pf} \frac{\partial T_f}{\partial t} + \rho_f C_{pf} v_{fr} \frac{\partial T_f}{\partial z} - \lambda_f \frac{\partial^2 T_f}{\partial z^2} - \frac{\lambda_f}{r} \frac{\partial}{\partial r} \left( \frac{1}{r} \frac{\partial T_f}{\partial r} \right) = 0 \quad (18)$$

$$\rho_r C_{pr} \frac{\partial T_r}{\partial t} - \lambda_r \frac{\partial^2 T_r}{\partial z^2} - \frac{\lambda_r}{r} \frac{\partial}{\partial r} \left( \frac{1}{r} \frac{\partial T_r}{\partial r} \right) = 0 \quad (19)$$

Note, that for the “multichannel” fracture geometry, symmetry through the center of the tubes was assumed. It would be interesting to complete this research by considering channels radiating outward and giving increasing distance between channels with increasing travel distance from the well. Nevertheless, such a complex conceptualization would involve more parameters, and is beyond the scope of this work. As for the “parallel plate” model, heat and flux continuity is ensured at the interface between fracture and rock matrix.

## 4. Field Site and Experimental Setting

Push-pull heat tracer tests were conducted at the Ploemeur experimental site in Brittany, France (H+ network of experimental sites [hplus.ore.fr/en](http://hplus.ore.fr/en)). The experimental site is located in a fractured crystalline basement aquifer. It has been subject of several field investigations, including borehole geophysics, flowmeter logging, straddle packer tests [Le Borgne et al., 2007], hydrogeophysical surveys [Dorn et al., 2012], temperature measurements [Klepkova et al., 2011, 2014], fiber optic distributed temperature sensing (FO-DTS) measurements [Read et al., 2013, 2014]. The B1 borehole at the Ploemeur field site, where heat tracer tests were conducted, was found to be intersected by 3–5 flowing fractures with overall hydraulic transmissivities on the order of  $10^{-3}$  m<sup>2</sup>/s over the borehole length [Le Borgne et al., 2007; Klepkova et al., 2014]. This borehole

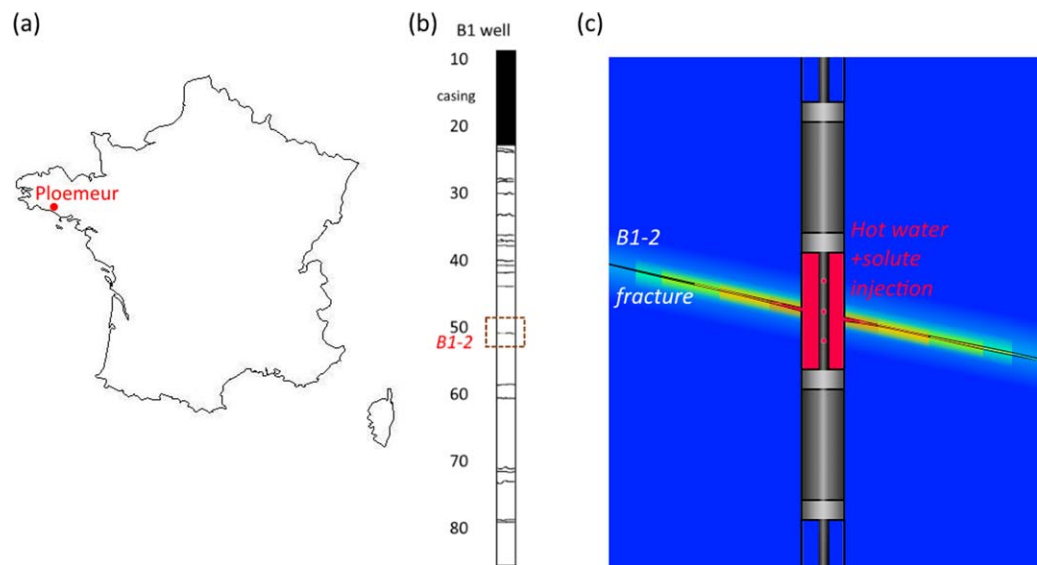


**Figure 4.** (a) Location of the Ploemeur field site, France. (b) Fracture traces measured in B1 borehole on optical and acoustic logs. Only the fractures interpreted as open from the image logs are represented (from *Le Borgne et al.* [2007]). (c) Experimental schema of a push-pull tracer test in B1-2 fracture (50.9 m depth) isolated with packers. Tracer injection as well as monitoring of temperature and conductivity were located in the middle of the double-packer system.

has been fully cored and in order to reduce uncertainties, we performed laboratory thermal analysis on the core samples. According to this analysis, the average granite bulk density, specific heat and thermal conductivity are the following:  $\rho_r = 2470 \text{ kg/m}^3$ ,  $C_{pr} = 738 \text{ J/kgK}$ ,  $\lambda_r = 3.31 \text{ W/mK}$ .

A series of heat push-pull tracer test were performed on the site following the schematic representation of Figure 4c. The experiments have been conducted in B1-2 fracture (Figure 4b), intersecting the B1 borehole at 50.9 m depth [*Le Borgne et al.*, 2007; *Dorn et al.*, 2012; *Read et al.*, 2013]. For each experiment, hot water was injected during the time interval  $t_{inj}$  at a controlled flow rate  $Q = 7 \text{ L/min}$  into the B1-2 fracture isolated from the rest of the injection borehole by a double-packer system (Figure 4c). The water was injected from a water tank at the surface, where a water heater (Swingtec Aquamobile DH6) was installed in order to maintain the temperature of injection at about  $50^\circ\text{C}$  (while the ambient groundwater temperature is about  $15^\circ\text{C}$ ). Due to the heat losses along the injection tubes, the temperature of injected hot water in-between the packers was around  $T_{inj} = 30^\circ\text{C}$ . In-situ measurements of temperature and conductivity were made with the CTD-Diver data logger (Schlumberger Water Services) located in the middle of the packers. The probe has a temperature accuracy of  $\pm 0.1^\circ\text{C}$ , a temperature resolution of  $0.01^\circ\text{C}$  with a response time of  $\sim 1 \text{ min}$ , a conductivity accuracy of  $10 \mu\text{S/cm}$  and a conductivity resolution of  $1 \mu\text{S/cm}$ . After the injection, we continued to push the tracer with fresh groundwater at approximately the same rate during the same time  $t_{push} = t_{inj}$ . Temperature, pressure and conductivity were monitored in the middle of the double-packer system. Direct measurements of ambient flow in B1-2 fracture were obtained at the experimental site using the finite volume point dilution method performed by *Jamin et al.* [2015]. The measured ambient flow was found to be below the detection limit ( $0.006 \text{ L/min}$ ), suggesting that ambient flow is too small to affect flow field created by the push-pull tests ( $7 \text{ L/min}$ ). Technical details of these tracer tests, referred to as Test 1,

Test 2, and Test 3, are synthesized in Table 1. By changing the injection duration, different volumes of rock were investigated.

**Table 1.** Experimental Setup of the Three Tracer Migration Experiments in B 1 – 2

Experimental Parameters	Experiment		
	Test1	Test2	Test3
Injection rate $Q$ , L/min	7	7	7.3
Duration of injection $t_{inj}$ , min	10	17	147
Maximum injection temperature $T_{inj}$ , $^\circ\text{C}$	33	34	27
Tracer conductivity $s$ , $\mu\text{S/cm}$	670	4000	670

## 5. Results

In this section, we discuss numerical and experimental results that reveal

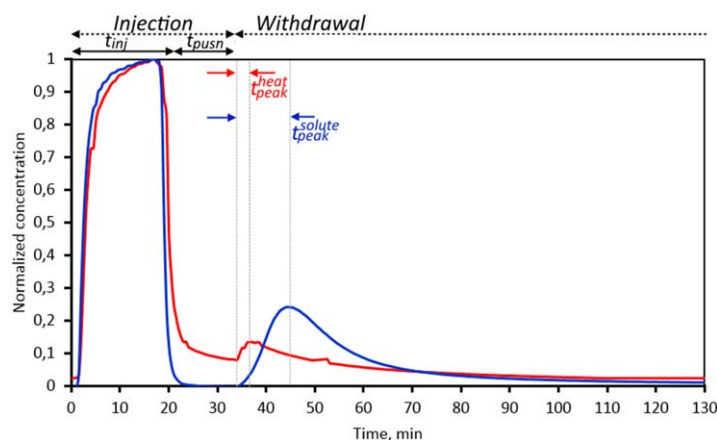


**Figure 5.** Temperature (red line) and concentration (blue line) breakthrough curves measured in between packers for Test 2. Concentrations are renormalized in order to have the same maximum value.

tion of the flushing fluid starts, both temperature and concentration drops down to their initial values. Note, that the temperature of flushing water was slightly higher than the groundwater temperature. After injecting a given chasing volume, the pump is reversed and an increase of conductivity and a lesser increase of temperature are observed.

For conservative, nonreacting solute push-pull tracer tests the time at which the maximum concentration peak is measured depends only on the experimental setup and equals to  $t_{peak}^{solute} = t_{push} + t_{pull}$  (time after injection) [Le Borgne and Gouze, 2008b]. The comparison of solute and temperature recovery shows that the temperature recovery peak arrives earlier than the concentration peak  $t_{peak}^{heat} < t_{peak}^{solute}$ . Moreover, the temperature peak is significantly smaller than the conductivity peak and the breakthrough curve exhibits a longer tailing. In the following section we demonstrate that these differences between solute and thermal breakthrough curves imply a greater sensitivity of heat push-pull tests to medium properties (fracture aperture and fracture geometry).

## 5.2. Sensitivity Analysis From Numerical Simulations

To understand the factors that control heat recovery in terms of peak amplitude, peak time and tailing, we present here a sensitivity analysis based on the numerical simulations presented in section 3. The parameters tested are: the flow rate, the fracture aperture and the fracture geometry (plane, channel or multichannel geometries).

### 5.2.1. Sensitivity of Heat Recovery to Flow Rate and Fracture Aperture

As demonstrated by Jung and Pruess [2012], the injection flow rate is not expected to impact the thermal breakthrough curves in push-pull tests. While flow influences the temperature distribution in the push phase, this effect is compensated exactly in the pull phase. This is confirmed from our numerical simulations for both the “parallel plate” and “channel models.” In order to study the influence of the fracture aperture on temperature recovery, we conducted a series of numerical tests where the fracture aperture was varied from 0.5 to 30 mm, while the flow rate was fixed to  $Q=7$  L/min and the injection and push times were fixed to  $t_{push} = t_{inj} = 10$  min. These conditions are identical to the experimental conditions of Test 1. Temperature breakthrough curves for varying fracture aperture are presented in Figures 6a and 6b for the “plate” and “channel” fracture geometries respectively. Test 1 experimental data are presented in the same plot for comparison (black dashed line).

For both fracture geometries (Figures 6a and 6b) an increase of fracture aperture leads to an increase in the amplitude of the thermal breakthrough curve peak. As the thermal tracer is pushed in the fracture, the heat which has diffused across the fracture diffuses away into the matrix. An increase of fracture aperture implies that heat needs more time to diffuse across the fracture aperture thus decreasing the heat diffusion length-scale for a given time of testing. During the backflow, heat is transferred back from the matrix into the fracture, the further the matrix heat plume has diffused during the push phase, the lower is the back thermal flux expected to be during the pull phase. Consequently, larger fracture apertures imply less heat loss to

the sensitivity of the thermal breakthrough curve to fracture geometry and demonstrate the scaling laws that control heat transfer in fractured media.

### 5.1. Comparison of Solute and Thermal Breakthrough Curves

An example of a measured push-pull thermal breakthrough curve is presented in Figure 5. All the breakthrough curves presented in this study are normalized to integrate to 1. During the experiment (Test 2) presented in Figure 5, salt, as a conservative tracer, was added during fluid injection (Table 1). Once injection

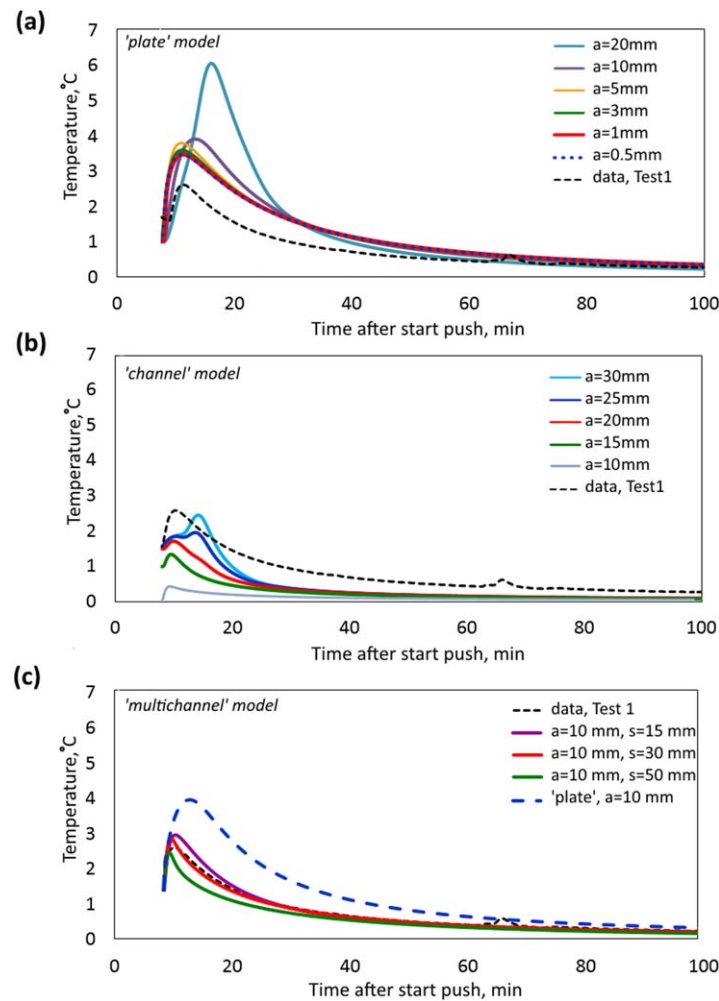


**Figure 6.** Effect of changes in fracture aperture on temperature breakthrough curve for (a) “plate” and (b) “channel” fracture models. (c) Effect of changes in fracture separation distance for “multichannel” model. Experimental data from Test 1 are given for comparison (black dashed line).

the matrix. Note that as the injection time is increased, thus increasing the heat diffusion length scale, the differences between the temperature breakthrough curves for different fracture apertures become less distinct. For the “plate” fracture model (Figure 6a) thermal breakthrough curves become insensitive to aperture for apertures  $a \leq 5$  mm, which is in agreement with the results of Jung and Pruess [2012]. Furthermore, the peak arrival time is found to increase with increasing fracture aperture (see also Figure 9). The sensitivity of peak time to fracture aperture represents a fundamental difference with conservative, nonreacting solute push-pull tracer tests, for which the peak time depends only on the experimental set up (i.e., push time and injection time) and not on the medium properties. This greater sensitivity of heat push-pull tests to medium properties indicates that they may provide complementary information to solute push-pull tests.

### 5.2.2. Sensitivity of Heat Recovery to Fracture Geometry

To understand the impact of fracture geometry on heat recovery,

we analyze the modeled temperature fields for both the “plate” and “channel” models with equals fracture apertures  $a = 10$  mm and a flow rate fixed to  $Q=7$  L/min (Figure 7). The temperature distribution at fracture walls (Figure 7a) for the same time (here time corresponds to the end of the injection period for Test 1  $t = t_{inj}$ ) is shown in Figure 7b for the “plate” (red line) and for “channel” (blue line) fracture models. This result shows that due to rapid heat transfer from the rock mass to the “channel” fracture, fracture walls are heated only in the vicinity of the injection point at  $r = 0$ , while a “plate” fracture allows advecting heat plume further away from the borehole. Hence, in thermal push-pull tests, the “channel” fracture is more efficient in exchanging heat between fracture and matrix than the “plate” fracture. The reason is that the diffusive flux from the fracture to the matrix (or vice versa) is two-dimensional in the “channel” fracture, while it is one-dimensional in the “plate” fracture.

Once the pull phase starts, water in the fracture then flows back and extracts the heat from the rock. For the “channel” model the heat reaches its peak value almost simultaneously with the start of pumping while for the “plate” fracture heat travels larger distance back thus increasing the peak arrival time. Note, that the distance at which the heat plume propagates increases with increasing fracture aperture, thus slowing down the peak arrival during the pull phase of testing. It is also worth remarking that the maximum distance covered by the heat plume is directly related to the injection flow rate and by increasing the flow rate the volume of the investigated by the tracer media can be increased.

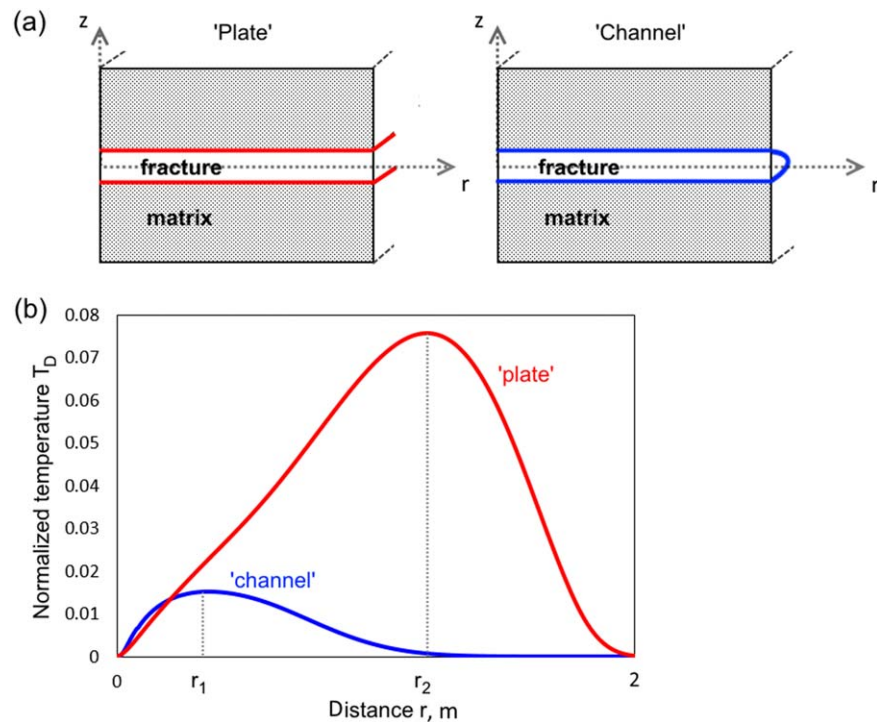


**Figure 7.** (a) Temperature distribution at the end of the injection period for (left) “plate” and for (right) “channel” (right) fracture models. (b) Temperature profiles at the fracture wall at the end of the injection period for “plate” (red) and for “channel” (blue) fracture models. Conditions of the numerical experiment correspond to the conditions of Test 1, the aperture of  $a = 10$  mm is considered in both simulations. Temperature is normalized to the injection temperature.

For strongly channeled flow in a fracture, it is likely that multiple channels exist in a fracture plane and may exchange heat between each other. In order to investigate heat transport through multiple flowing channels we studied how the number of flowing channels, their separation distance as well as the distribution of channel flow velocities may affect thermal breakthrough curves. The fracture aperture of each single channel was fixed at  $a = 10$  mm. As expected, neighboring channels exchange heat between each other (Figure 2b). When hot water is injected into channels, the heat plume propagates from fractures into the matrix and after a certain time reaches neighboring channels. Through this mechanism, the heat that is lost to the matrix by some channels can be recovered by other channels. This enhances the recovered temperature signal as shown in Figure 6c. As the distance between channels increases, this process becomes less efficient and thus the recovered temperature decreases when the distance between channels increases. When the separation distance  $s$  becomes larger than the characteristic diffusion scale over the experiment time  $s_D = \sqrt{2D_r t_{push}}$  neighboring channels do not exchange heat anymore, and recovered breakthrough curves are identical to those obtained with a single “channel” model. Here  $D_r = \frac{\lambda_r}{\rho_r c_{pr}}$  refers to the rock thermal diffusivity. For the conditions of our test this characteristic distance equals  $s_D \simeq 400$  mm. For more than eight channels with a given aperture the recovered temperature signal was found to be independent of the number of channels.

### 5.3. Interpretation of a Single Thermal Push-Pull Test

In this section, we compare the measured thermal breakthrough curve from Test 1 with the simulated breakthrough curves obtained for the different fracture geometries discussed above. We seek a model able to reproduce both the peak amplitude and peak time.

The “plate” model was found to overestimate the amplitude of thermal breakthrough curves for all tested fracture apertures (Figure 6a). The simulated peak time is compatible with the data for apertures less than 5 mm. The mismatch in recovered amplitude may be explained by the limited efficiency of heat diffusion in the “plate” model. The “channel” model on the other hand predicts much smaller heat recovery since radial heat diffusion is more efficient for the same volume of injected heated fluid (Figure 6b). However, with a

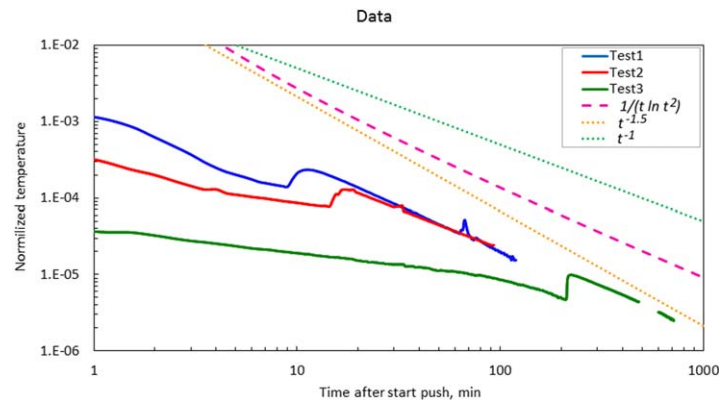


**Figure 8.** Breakthrough curves for push-pull heat tracer tests in B1 – 2 fracture. Here temperature is normalized so that its integral, over injection and pushing time, is 1.

single channel it is not possible to match both the peak amplitude and the peak time. This can be achieved by considering multiple channels. For a given peak time, the peak amplitude can be adjusted by varying the mean distance between channels. Hence, given that a “channel” model with the fracture aperture  $a = 10$  mm provides a good fit to the data in terms of peak arrival time, we considered a “multichannel” model with  $a = 10$  mm and varying separation distance  $s = 15$  to 50 mm.

The best match with the breakthrough curve from Test 1 was provided by the “multichannel” fracture model with  $a = 10$  mm aperture channels separated by  $s = 30$  mm distance (Figure 6c). Although no detailed aperture distributions are available for the fractures at the Ploemeur site, evidence from previous solute tracer tests [Kang et al., 2015] suggests that fracture apertures at the site are expected to be relatively large, around few mm or even the cm, meaning that our test yields a reasonable estimate of the aperture. This result confirms that thermal push-pull tests are complementary to conservative, nonreacting solute push-pull tests in terms of sensitivity and thus can provide rich information on the medium properties. In the following section we investigate the relevance of the multichannel model for modeling heat recovery at different scales.

## 5.4. Scale Effects in Peak Temperature Recovery and Peak Arrival Time

### 5.4.1. Experimental Results

To explore the scale dependence of the thermal recovery, three thermal push-pull tests with injection times  $t_{inj}$  of 10, 17 and 147 min were conducted. As expected, the recovered peak temperature is found to decrease with the scale of investigation (Figure 8). The peak temperature is found to scale approximately as  $T_{peak} \propto t^{-1}$ .

### 5.4.2. Numerical Results

In order to study the relevance of different fracture models across scales, we examine the scale dependency of the peak amplitude and peak time with a single set of parameters. Predictions of the three models described in the previous section are compared to the measured peak amplitudes (Figure 9a) and peak arrival times (Figure 9b). The fracture aperture is fixed as  $a = 10$  mm for “plate,” “channel” and “multichannel” models. For the “multichannel” model, channels are separated by  $s = 30$  mm distance. For the peak amplitude, the multiscale results confirm that the “plate” model tends to systematically over-estimate the heat recovery, while the single “channel” model tends to underestimate it. The “multichannel” model provides good predictions at all investigated scales for the peak amplitude. For the peak time, the “plate” model is found to diverge from the data at large scale, while the mismatch for the single “channel” and for the “multichannel” does not exceed few minutes and appears to be independent on scale. These results suggest that the “multichannel” model is robust and provides reliable predictions with a limited set of parameters.

## 5.5. Late Time Behavior of Thermal Breakthrough Curves

### 5.5.1. Experimental Results

The measured thermal breakthrough curves show strong tailing, which is consistent at all scales and close to  $T(t) \propto t^{-1}$ . Since the logarithmic correction has a weak effect on the considered time scales, this tailing turns out to be close to  $T(t) \propto \frac{1}{t \ln(t)^2}$ , the scaling behavior we find through theoretical developments for heat recovery from a channel (section 2.2). This agrees very well with a model of heat recovery in a channel.

This observation contrasts with the tailing observed from solute tracer tests on the same fracture, that showed power law behavior  $c(t) \propto t^{-\beta}$ , with an exponent ranging from  $\beta = 1.75$  for cross-borehole tracer tests to  $\beta = 2.5$  for push-pull tests [Kang et al., 2015]. These exponents were successfully explained from a

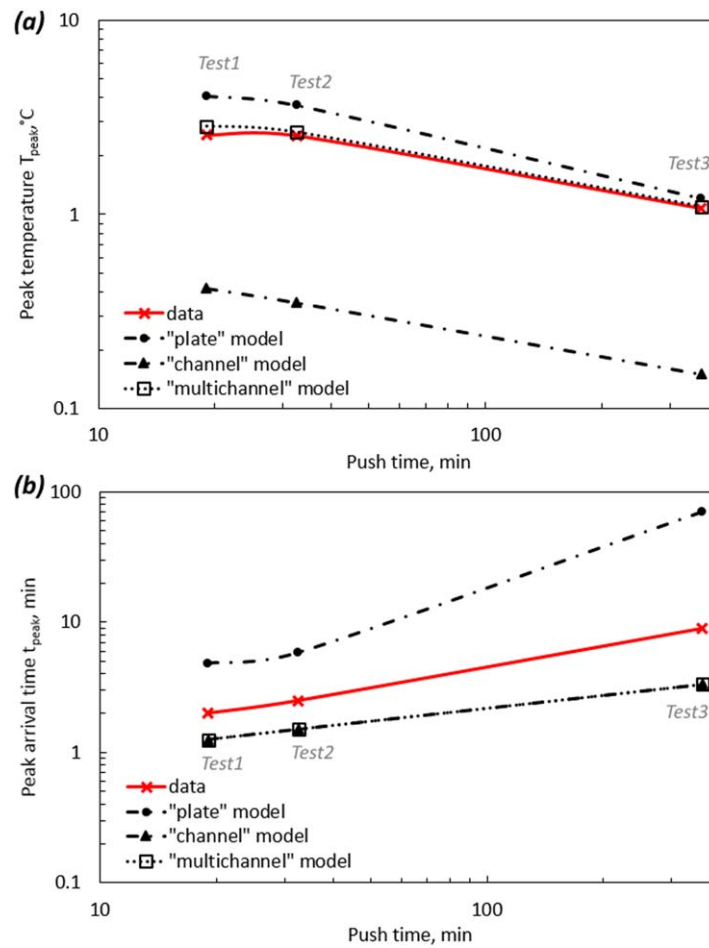


**Figure 9.** Effect of scale on (a) temperature peaks and (b) temperature peak arrival times. Comparison of experimental data (red line with crosses) and results of numerical modeling for a “plate” model with fracture aperture  $a = 10$  mm (black dashed-dotted line with circles), “channel” model with fracture aperture  $a = 10$  mm (black dashed line with triangles) and “multichannel” fracture model with fracture aperture  $a = 10$  mm and fracture separation distance  $s = 30$  mm (black dotted line with squares).

predictions of the “multichannel” model, obtained with a single set of parameters, are therefore fully consistent with the whole data set.

## 6. Conclusions

The scaling theory and experimental data set presented in this study provides new insights on heat transfer in fractured media. These findings question the relevance of the classical parallel plate model for modeling heat transfer in fractured media. Channeled flow is shown to have a clear signature on the scale dependency of heat recovery, which can be measured from the peak amplitude and peak arrival time of thermal breakthrough curves at different scales. Radial diffusive fluxes in the channel model are more efficient for transmitting heat to the matrix and less efficient for recovering it compared to the parallel plate model.

The impact of channeled flow on heat diffusion is manifested in the temporal decay of temperature at late time, which does not follow the classical diffusive scaling  $t^{-1.5}$ . While the latter scaling is generally considered to be independent of the immobile zone geometry, we show here that it breaks down for mobile channels embedded into an immobile matrix. The temporal scaling of late time breakthrough curves is shown to depend on the dimensionality of diffusive fluxes from the immobile to the mobile domain. This translates into a scaling of late time breakthrough curves such as  $T(t) \propto \frac{1}{\ln t^2}$  for the

correlated Continuous Time Random Walk (CTRW) model quantifying variability in fracture aperture (velocity distribution) and connectedness of flow channels in the fracture plane (velocity correlation). The tailing observed in the thermal breakthrough curves is thus much more pronounced than for solute breakthrough curves measured at the same location. Solute tailing is mainly due to heterogeneous advection and diffusion within the fracture plane since solute diffusion into the matrix is negligible for the considered granite rock.

### 5.5.2. Numerical Results

Our theoretical investigations imply that the plate and channel models are expected to differ in terms of breakthrough curve tailing. In order to confirm this finding numerical simulations were conducted. Modeling results are then presented in log-log in Figure 10, and experimental data are given in the same figure for comparison (black dashed line). As expected, the “plate” models produce breakthrough tailing such as  $T(t) \propto t^{-3/2}$ , while “channel” and “multichannel” models produce a stronger tailing such as  $T(t) \propto \frac{1}{\ln(t)^2}$ . The

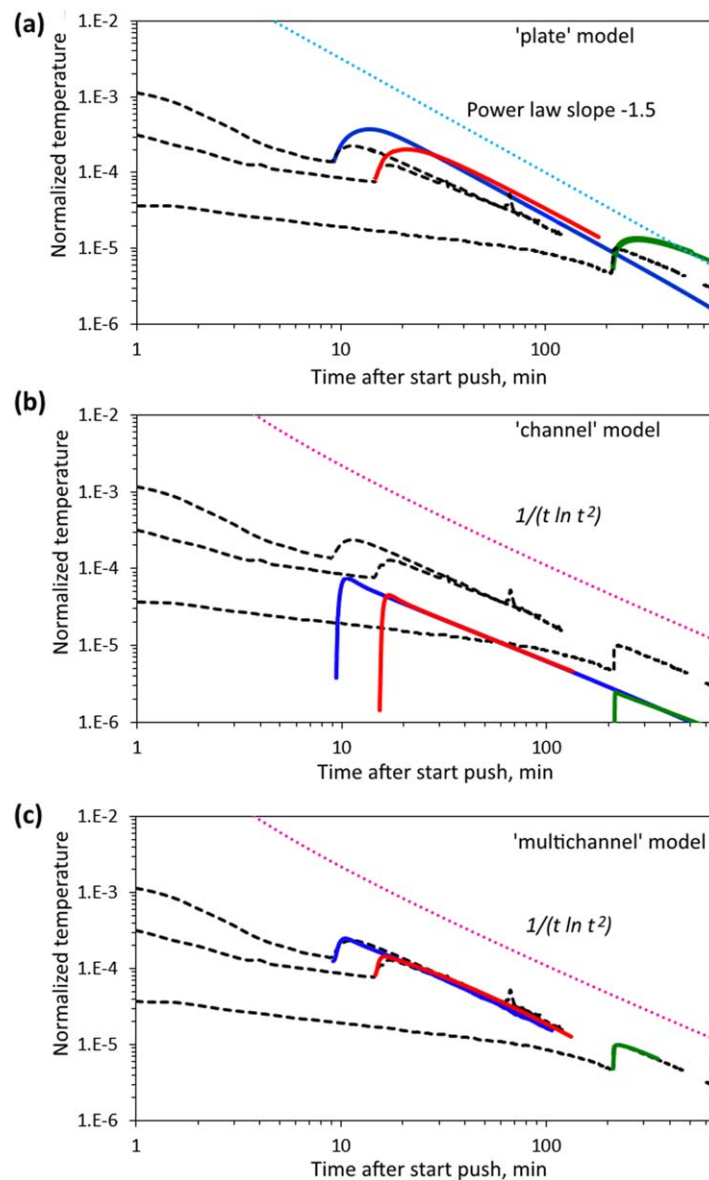


**Figure 10.** Effect of scale on temperature breakthrough curves. Comparison of experimental data (black dashed line) and results of numerical modeling (blue line—Test 1, red line—Test 2, green line—Test 3) for a (a) “plate,” (b) “channel” and (c) “multichannel” fracture models.

channel model. As this scaling was consistently apparent for our experiments at all investigated scales, we conclude that matrix diffusion is strongly controlled by channeled flow at the considered experimental site.

Channeled flow was also observed at the same site from independent measurements of a different nature. Kang *et al.* [2015] explained the difference in tailing behavior observed in solute tracer tests in cross-borehole and push-pull conditions performed on the same fracture by the existence of a characteristic velocity correlation length of about 40 cm, which may be due to channeled flow inside fractures. Furthermore, Shakas *et al.* [2016] estimated the mean tracer position as a function of time from GPR imaging of tracer motion in push-pull conditions in the same fracture. They observed a linear behavior of the mean radial position with time until a distance  $r = 2$  m, which points to the existence of channeled flow below this characteristic distance.

The results of this study have shown that thermal push-pull tests provide complementary information compared to solute push-pull tests since the peak amplitude, the analysis of the scale dependency of

the peak time and the temporal decay of heat recovery provides meaningful information that is not contained in solute push-pull breakthrough curves. A multichannel model with a single set of parameters was able to represent the whole thermal push-pull data set, which is encouraging regarding the possibility to define reliable models for heat transfer in fractured media. Push-pull thermal tracer tests thus appears to be a promising approach for characterizing fractured media since they provide insights into fracture shape and aperture, which is generally difficult to obtain under in-situ conditions at field-scale.

The derivation of temporal and spatial scaling laws for heat recovery in channeled fractures may have significant applications for modeling heat storage and geothermal applications. Furthermore, the demonstration of the impact of channeled flow on matrix diffusion may have important implications for modeling solute transfer in fractured porous media where breakthrough curve tailing may be governed by the interplay between fracture flow channeling and matrix diffusion.

### Acknowledgments

The fieldwork data in this study are available from the authors upon request (maria.klepikova@erdw.ethz.ch). This work was supported by the European Marie Curie network IMVUL (grant agreement 212298), by the National Research Observatory H+ and by the European Interreg IV project CLIMAWAT and the ANR project Stock en socles. We also thank Alain Dassargues and Serge Brouyeres from the University of Liege, Belgium for their kind assistance in providing a water heater. MD acknowledges the support of the European Research Council (ERC) through the project MHetScale (617511).

### References

- Abramowitz, M., and I. Stegun (1972), *Handbook of Mathematical Functions With Formulas, Graphs, and Mathematical Tables*, John Wiley, N. Y.
- Anderson, M. P. (2005), Heat as a ground water tracer, *Ground Water*, 43(6), 951–968.
- Becker, M. W., and A. M. Shapiro (2000), Tracer transport in fractured crystalline rock: Evidence of nondiffusive breakthrough tailing, *Water Resour. Res.*, 36(7), 1677–1686.
- Becker, M. W., and A. M. Shapiro (2003), Interpreting tracer breakthrough tailing from different forced-gradient tracer experiment configurations in fractured bedrock, *Water Resour. Res.*, 39(1), 1024, doi:10.1029/2001WR001190.
- Bodvarsson, G. S., and C. F. Tsang (1982), Injection and thermal breakthrough in fractured geothermal reservoirs, *J. Geophys. Res.*, 87(B2), 1031–1048.
- Carrera, J., X. Sánchez-Vila, I. Benet, A. Medina, G. Galarza, and J. Guimerà (1998), On matrix diffusion: Formulations, solution methods, and qualitative effects, *Hydrogeol. J.*, 6, 178–190.
- Comolli, A., G. Hidalgo, C. Moussey, and M. Dentz (2016), Non-Fickian transport under heterogeneous advection and mobile-immobile mass transfer, *Transp. Porous Media*, 1–25, doi:10.1007/s11242-016-0727-6.
- Dentz, M., and B. Berkowitz (2003), Transport behavior of a passive solute in continuous time random walks and multirate mass transfer, *Water Resour. Res.*, 39(5), 1111, doi:10.1029/2001WR001163.
- Dentz, M., P. K. Kang, and T. Le Borgne (2015), Continuous time random walks for non-local radial solute transport, *Adv. Water Resour.*, 82, 16–26.
- Dorn, C., N. Linde, T. Le Borgne, O. Bour, and M. Klepikova (2012), Inferring transport characteristics in a fractured rock aquifer by combining single-hole gpr reflection monitoring and tracer test data, *Water Resour. Res.*, 48, W11521, doi:10.1029/2011WR011739.
- Geiger, S., and S. Emmanuel (2010), Non-Fourier thermal transport in fractured geological media, *Water Resour. Res.*, 46, W07504, doi:10.1029/2009WR008671.
- Genter, A., L. Guillou-Frottier, J.-L. Feybesse, N. Nicol, C. Dezayes, and S. Schwartz (2003), Typology of potential hot fractured rock resources in Europe, *Geothermics*, 32, 701–710.
- Gouze, P., Y. Melean, T. Le Borgne, M. Dentz, and J. Carrera (2008a), Non-Fickian dispersion in porous media explained by heterogeneous microscale matrix diffusion, *Water Resour. Res.*, 44, W11416, doi:10.1029/2007WR006690.
- Gouze, P., T. Le Borgne, R. Leprovost, G. Lods, T. Poidras, and P. Pezard (2008b), Non-Fickian dispersion in porous media: 1. Multiscale measurements using single-well injection withdrawal tracer tests, *Water Resour. Res.*, 44, W06426, doi:10.1029/2007WR006278.
- Gringarten, A. C., and J. P. Sauty (1975), A theoretical study of heat extraction from aquifers with uniform regional flow, *J. Geophys. Res.*, 80(35), 4956–4962.
- Gylling, B., L. Moreno, and I. Neretnieks (1999), The Channel Network Model - A Tool for Transport Simulations in Fractured Media, *Ground Water*, 37(3), 367–375, doi:10.1111/j.1745-6584.1999.tb01113.x.
- Hadermann, J., and W. Heer (1996), The Grimsel (Switzerland) migration experiment: Integrating field experiments, laboratory investigations and modelling, *J. Contam. Hydrol.*, 21(1–4), 87–100.
- Haggerty, R., and S. M. Gorelick (1995), Multiple-rate mass transfer for modeling diffusion and surface reactions in media with pore-scale heterogeneity, *Water Resour. Res.*, 31(10), 2383–2400.
- Haggerty, R., S. A. McKenna, and L. C. Meigs (2000), On the late-time behavior of tracer test breakthrough curves, *Water Resour. Res.*, 36(12), 3467–3479.
- Haggerty, R., S. Fleming, L. C. Meigs, and S. A. McKenna (2001), Tracer tests in a fractured dolomite 2. analysis of mass transfer in single-well injection-withdrawal tests, *Water Resour. Res.*, 37(5), 1129–1142.
- Hosanski, M., and E. Ledoux (1982), In situ determination of the hydrothermal properties of a deep fractured medium by a single-well technique, *J. Hydrol.*, 56(1–2), 39–47.
- Incropera and DeWitt (1996), *Fundamentals of Heat and Mass Transfer*, fourth ed., John Wiley and Sons, N. Y.
- Irvine, D. J., C. T. Simmons, A. D. Werner, and T. Graf (2015), Heat and solute tracers: How do they compare in heterogeneous aquifers?, *Ground Water*, 53, 10–20.
- Jamin P, P. Goderniaux, O. Bour, T. Le Borgne, A. Englert, L. Longuevergne, and S. Brouyère (2015), Contribution of the finite volume point dilution method for measurement of groundwater fluxes in a fractured aquifer, *J. Contam. Hydrol.*, 182, 244–255.
- Jung, Y., and K. Pruess (2012), A closed-form analytical solution for thermal single-well injection-withdrawal tests, *Water Resour. Res.*, 48, W03504, doi:10.1029/2011WR010979.
- Kang, P. K., T. Le Borgne, M. Dentz, O. Bour, and R. Juanes (2015), Impact of velocity correlation and distribution on transport in fractured media: Field evidence and theoretical model, *Water Resour. Res.*, 51, 940–959, doi:10.1002/2014WR015799.
- Klepikova, M., T. Le Borgne, O. Bour, and P. Davy (2011), A methodology for using borehole temperature-depth profiles under ambient, single and cross-borehole pumping conditions to estimate fracture hydraulic properties, *J. Hydrol.*, 407, 145–152, doi:10.1016/j.jhydrol.2011.07.018.
- Klepikova, M., T. Le Borgne, O. Bour, K. Gallagher, R. Hochreutener, and N. Lavenant (2014), Passive temperature tomography experiments to characterize transmissivity and connectivity of preferential flow paths in fractured media, *J. Hydrol.*, 512, 549–562, doi:10.1016/j.jhydrol.2014.03.018.
- Kocabas, I. (2005), Geothermal reservoir characterization via thermal injection backflow and interwell tracer testing, *Geothermics*, 34, 27–46.
- Kocabas, I., and R. N. Horne (1990), A new method of forecasting the thermal breakthrough time during reinjection in geothermal reservoirs, paper presented at Fifteenth Workshop on Geothermal Reservoir Engineering, Stanford University, Stanford, Calif.
- Kolditz, O. (1995), Modelling flow and heat transfer in fractured rocks: Dimensional effect of matrix heat diffusion, *Geothermics*, 24, 421–437.
- Lauwerier, H. A. (1955), The transport of heat in an oil layer caused by the injection of hot fluid, *Appl. Sci. Res., Sect. A*, 5, 145–150.
- Le Borgne, T., and P. Gouze (2008), Non-Fickian dispersion in porous media: 2. Model validation from measurements at different scales, *Water Resour. Res.*, 44, W06427, doi:10.1029/2007WR006279.
- Le Borgne, T., et al. (2007), Comparison of alternative methodologies for identifying and characterizing preferential flow paths in heterogeneous aquifers, *J. Hydrol.*, 345, 134–148.
- Maloszewski, P., and A. Zuber (1985), On the theory of tracer experiments in fissured rocks with a porous matrix, *J. Hydrol.*, 79(3–4), 333–358.
- Molson, J., P.E. Pehme, J. Cherry, and B. Parker (2007), Numerical analysis of heat transport within fractured sedimentary rock: Implications for temperature probes, paper presented at NGWA/U.S. EPA Fractured Rock Conference: State of the Science and Measuring Success in Remediation, 5017, pp. 489–502, Portland, Maine.

- Neretnieks, I. (2007), Single well injection withdrawal tests (swiw) in fractured rock: Some aspects on interpretation, *SKB Rapp. R-07-54, Dep. of Chem. Eng. and Technol., R. Inst. of Technol., Stockholm, Sweden*.
- Neuvillle, A., R. Toussaint, and J. Schmittbuhl (2010), Hydrothermal coupling in a self-affine rough fracture, *Phys. Rev. E*, *82*, 036317.
- Pruess, K., and C. Doughty (2010), Thermal single-well injection-withdrawal tracer tests for determining fracture-matrix heat transfer area, paper presented at Thirty-Fifth Workshop on Geothermal Reservoir Engineering, Rep No: LBNL-4211E, Stanford Univ., Stanford, Calif.
- Read, T., O. Bour, V. F. Bense, T. Le Borgne, P. Goderniaux, M. Klepikova, R. Hochreutener, N. Lavenant and V. Boschero (2013), Characterizing groundwater flow and heat transport in fractured rock using fiber-optic distributed temperature sensing, *Geophys. Res. Lett.*, *40*, 2055–2059, doi:10.1002/grl.50397.
- Read, T., O. Bour, J. S. Selker, V. F. Bense, T. Le Borgne, R. Hochreutener, and N. Lavenant (2014), Active-distributed temperature sensing to continuously quantify vertical flow in boreholes, *Water Resour. Res.*, *50*, 3706–3713, doi:10.1002/2014WR015273.
- Redner, S. (2001), *A Guide to First-Passage Processes*, Cambridge Univ. Press, Cambridge.
- Saar, M. (2011), Review: Geothermal heat as a tracer of large-scale groundwater flow and as a means to determine permeability fields. *Hydrogeol. J.*, *19*(1), 31–52.
- Selker, J., L. Thvenaz, H. Huwald, A. Mallet, W. Luxemburg, N. van de Giesen, M. Stejskal, J. Zeman, M. Westhoff, and M. B. Parlange (2006), Distributed fiber-optic temperature sensing for hydrologic systems, *Water Resour. Res.*, *42*, W12202, doi:10.1029/2006WR005326.
- Shakas, A., N. Linde, L. Baron, O. Bochet, O. Bour and T. Le Borgne (2016), Hydrogeophysical characterization of transport processes in fractured rock by combining push-pull and single-hole ground penetrating radar experiments, *Water Resour. Res.*, *52*, 938–953, doi:10.1002/2015WR017837.
- Tsang, Y. W. (1995), Study of alternative tracer tests in characterizing transport in fractured rocks, *Geophys. Res. Lett.*, *22*(11), 1421–1424.
- Vogt, T., P. Schneider, L. Hahn-Woernle, and O. A. Cirpka (2010), Estimation of seepage rates in a losing stream by means of fiber-optic high-resolution vertical temperature profiling, *J. Hydrol.*, *380*(1-2), 154–164.